ESRF	**Experiment title:** Dimensional and single-atom effects on critical fluctuations of magnetic surfaces and thin films	**Experiment number**: HE-623
Beamline:	**Date of experiment**: from: September 1, 1999 to: September 1, 2001	**Date of report**: 26/03/02
Shifts:	**Local contact(s)**: Dr. N. Brookes, Dr. S. Dhesi, Dr. C. Detlefs	*Received at ESRF:*

Names and affiliations of applicants (* indicates experimentalists):

*Dr. J.B. Goedkoop, *J.F. Peters, *M.A. de Vries, *J. Miguel Soriano, *Dr. O. Toulemonde

Van der Waals – Zeeman Instituut, University of Amsterdam

REPORT LONG TERM PROPOSAL HE623

J.B. Goedkoop, J.F. Peters, M.A. de Vries, J.Miguel Soriano, O. Toulemonde
Van der Waals Zeeman Institute, University of Amsterdam, The Netherlands

Overview of activities

This report describes activities in the framework of the long-term proposal HE623 between September 1, 1999 and September 1, 2001. The proposal aimed at the development of dynamical x-ray scattering for the study of dynamical effects in magnetic surfaces, films and nanosystems. It was supported by a major grant from the Dutch Foundation for Fundamental Research on Matter (FOM) under the program "*Fundamental properties of surfaces and interfaces*" for the period September 1999 - September 2003 (1 PhD, 1 Post Doc and investments for the construction of a UHV diffractometer).
HE623 was allocated 36 shifts on ID10A and 72 shifts on ID12B/ ID08. An overview of the runs is given in the appendix. The program has been highly successful in the soft x-ray range, where we obtained the best magnetic diffraction and speckle results to date, as will be shown below. In the high-energy experiments on ID10A we successfully commissioned and characterized a new diamond quarter wave plate, but failed to obtain reliable magnetic diffraction results. However, the experience obtained in alignment and cleaning of the diffraction signal on ID10A proved instrumental for our successes in the soft x-ray range.

A preliminary report of this work has been given in the ESRF newsletter [1]. Since then a vast amount of detailed and high quality data have been gathered which are being worked out and will result in a thesis by J.F. Peters and several papers. Publications on magnetic diffraction and coherent magnetic scattering are under preparation and will be submitted in the coming months.

A preliminary account, reflecting the current state of data analysis is given in this report. Parts of these results were presented in 18 oral presentations and 9 poster presentations.
Our work has been hampered greatly since September 2001, when the Institute was confronted with an unexpected close-down on account of asbestos hazards. The situation is slowly normalizing, but still costs a large amount of effort and attention. Our scientific output has suffered badly from this situation, and we cannot but ask for the review committee's consideration of these problems.
The structure of this report is as follows: We first describe in some detail the magnetic structure of stripe domains in GdFe thin films, which were the main subject of study. Then we describe magnetic diffraction with partially coherent beams. Finally we discuss magnetic speckle experiments performed with coherent beams. An appendix gives an overview of the experimental runs.

Self-organized stripes in amorphous GdFe films

In order to understand the resonant scattering technique better, as well as to develop instrumentation we have devoted considerable effort on the study of stripe domains. Such stripe systems can exist in thin films with an out-of-plane microscopic crystal-field induced anisotropy, and is a result of the competition between this perpendicular anisotropy and the dipolar magnetostatic energy of the sample as a whole, which favors in-plane magnetization. This competition causes the magnetization to self-organize in up-down magnetized meandering stripes.
Stripe domains have been observed in many films with perpendicular anisotropy and offer a convenient test ground for micromagnetic theory [2]. For this work we have chosen the amorphous GdFe system for several reasons:

- The magnetic behavior of this ferrimagnetic system can be readily tuned by changing the composition or the thickness (e.g. Fig. 1)
- The resonant magnetic contribution to the scattering cross section is expected to be large at the Gd M_{45} and L_{23} edges
- One can compare the Gd and Fe resonances
- The amorphous structure is easy to grow on almost any substrate, including ultrathin Si_3N_4 windows, allowing transmission experiments.

We have performed a systematic study of this system using samples grown with our MBE system. About 80 films were produced and characterized using MOKE (Magneto-Optical Kerr Effect), MFM, RBS and XRD. From this large set of samples we selected the two systems with the shortest stripe periodicity: 40 nm thick films of $GdFe_3$ and $GdFe_5$. Such samples were grown on Si wafers and ultrathin Si_3N_4 windows, and capped with ~2 nm Al films to protect them from oxidation. The substrates and film surfaces had roughness smaller than 1 nm, and no scattering from the structure of the film has been observed.

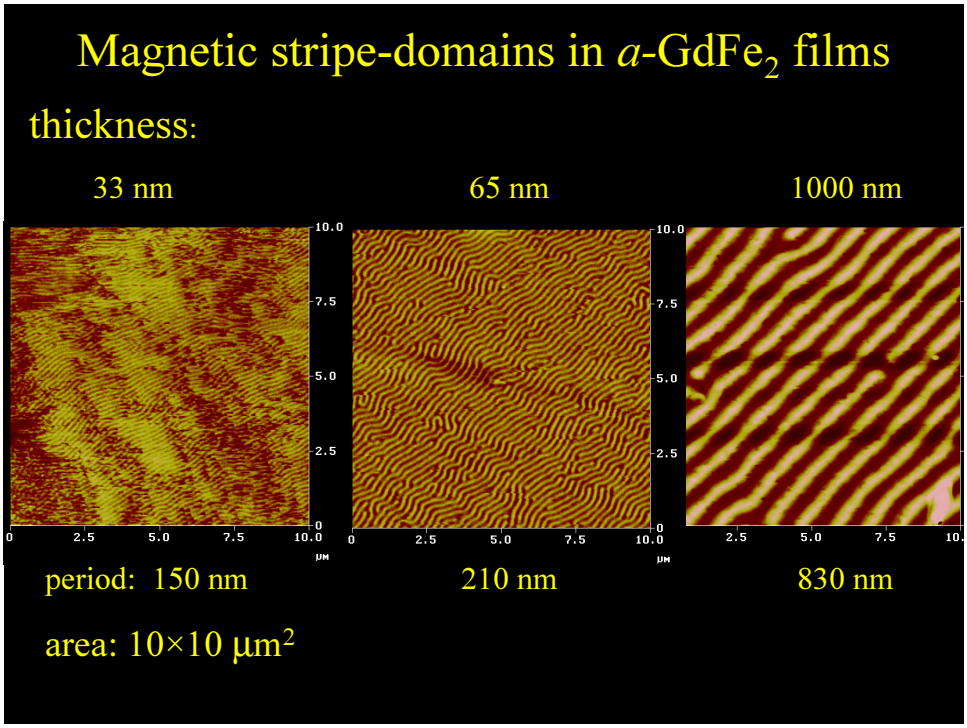

Fig. 1. MFM images of $GdFe_2$ films showing the dependence of the domain size on layer thickness at fixed composition.

Domain structure in amorphous films

The prototypical observation and description of stripe domains has been given by Kooij and Enz [3]. They used transmission magneto-optical Kerr microscopy to image domains in a slab of $BaFe_{12}O_{19}$ of 3 μm, and studied the effect of an applied field normal to the slab. Their theory accounts for the overall behavior of the magnetization loop, such as given in Fig. 2. On increasing the perpendicular field, initially in the *reversible region* the up domains grow at the expense of the down domains without changing the period. At higher fields, domain walls are depinned and the period increases. Near saturation the stripes are thought to degenerate in bubble domains, which collapse at sufficiently high fields. On decreasing the field the magnetization stays at the saturation value until reverse domains can nucleate. These rapidly expand and meander over the surface to a new stripe configuration.

The details of the magnetization distribution are quite complicated. Between each up and down domain pair one finds a Bloch wall in which the magnetization makes a gradual 180° transition by turning sideways. Near the surface the system tries to avoid free magnetic poles and the magnetization aligns itself parallel to the surface, forming closure domains as predicted by Kittel [4] (see Fig. 2b). Alternatively, the complete 3D structure can be thought of as an array of magnetic field vortices with alternating handedness. The pitch of the vortex depends on magnetization, anisotropy and thickness of the film. In principle such structures can be calculated by micromagnetic methods [2,5]. However, no experimental methods exist to verify such calculations with the required resolution. We will show below that magnetic resonant x-ray scattering is a powerful tool for experimental determination of the various vector components of the magnetization distribution.

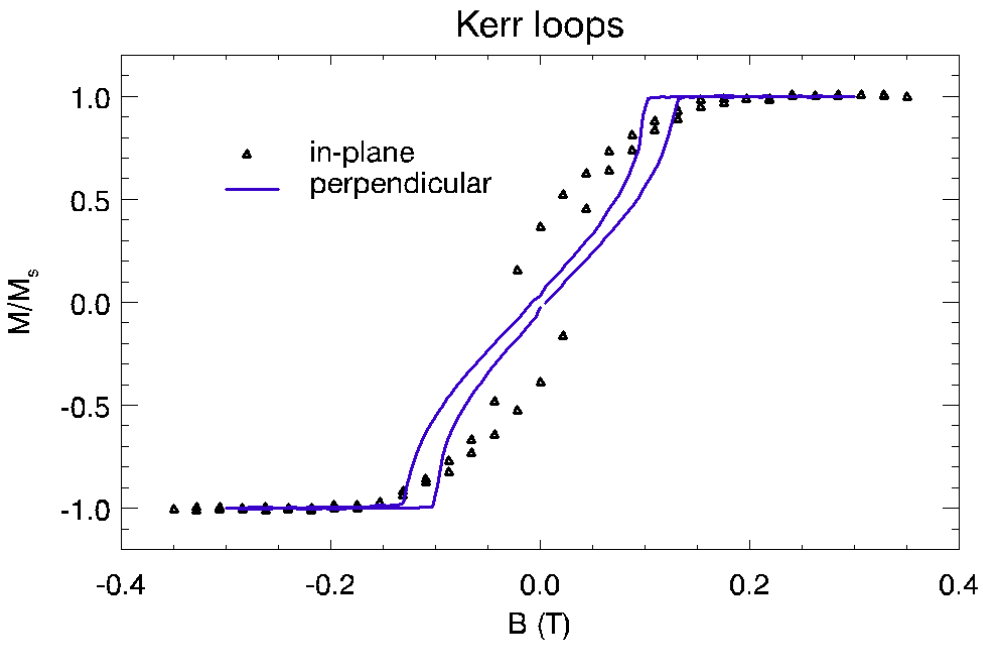

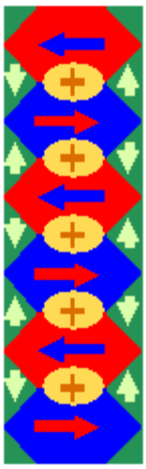

Fig. 2a. Magnetization loops of $GdFe_5$ for magnetic fields applied in the plane of the film (triangles) and normal to the film (full curve), as measured with transverse and polar MOKE.
Fig. 2b. Schematic representation of the stripe domain structure in thin films, showing primary stripe domains M_z (red and blue), Bloch walls M_y (orange +) and closure domains M_x (green).

Resonant soft x-ray scattering studies on stripe domains

The thickness of domain walls is measured in nanometers. Soft x-rays have 1 nm wavelengths in combination with strong magneto-optical contrast, and are compatible with high fields and low temperatures and therefore in principle are an ideal tool for domain structure studies. Indeed in this report we show that with XRMS one can obtain 3D structural information on length scales of ~10 nm, and follow the domain structure over the magnetization loop. We have used transmission and reflectivity geometries with a general layout as given in Fig. 3.
The experience of the Troika team convinced us that a 2D detector was vital for this program. Since no high efficiency in-vacuum soft x-ray CCD camera was available we developed a simple detector based on a phosphor coated window and a Sensicam CCD camera with appropriate optics. Two phosphors, P43 and P20, were tested. The latter turns out to have the higher yield and has a flatter response. It is slower with a larger afterglow, but for exposure times down to 1 ms this is not a problem.
This detector has several advantages over a direct exposure CCD camera: high dynamic range, 10 x higher lateral resolution (with microscope objective), sturdiness and flexibility: by changing the magnification of the optics we can readily trade *q*-resolution versus *q*-range, which proved to be extremely important for the resolution of magnetic speckle described.

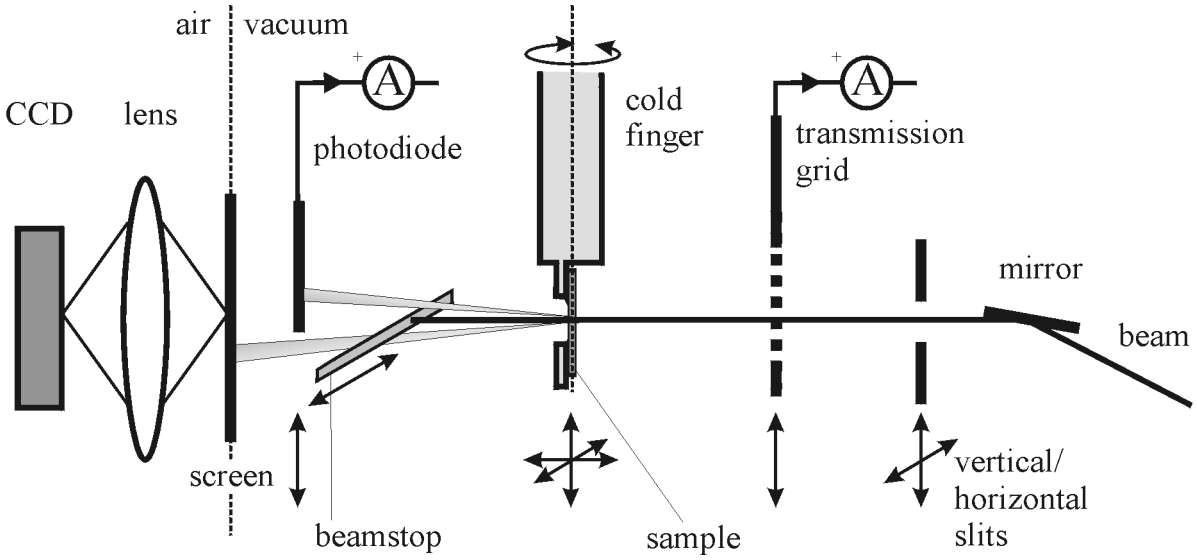

Fig. 3. General layout used in this work. The realization has gradually evolved from a simple optical rail concept to a full UHV diffractometer named Bertha, now stationed at ESRF.

As a typical example of our measurements we show in Fig. 4 the Gd M_{45} resonant diffraction patterns from ordered and disordered stripe systems. The disordered stripes are similar to an isotropic liquid of hard sphere particles, showing short-range order, and well-defined 1st and 2nd order diffraction rings are visible. After saturating the sample in a horizontal in-plane field, the stripes reconstruct in a highly ordered one-dimensional lattice, which produces a series of intense diffraction spots. Each 1st order spots contains 10% of the transmitted beam intensity and can indeed be observed by eye on the scintillator screen.

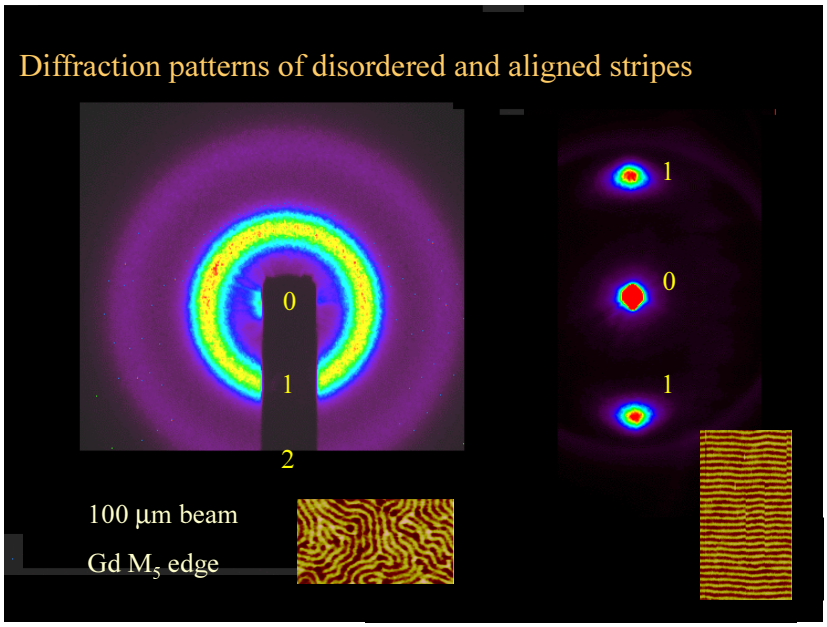

Fig. 4 Left: diffraction pattern from disordered stripes in $GdFe_5$ as shown in the MFM image taken in transmission at the Gd M_5 edge. Right: diffraction pattern of aligned stripes.

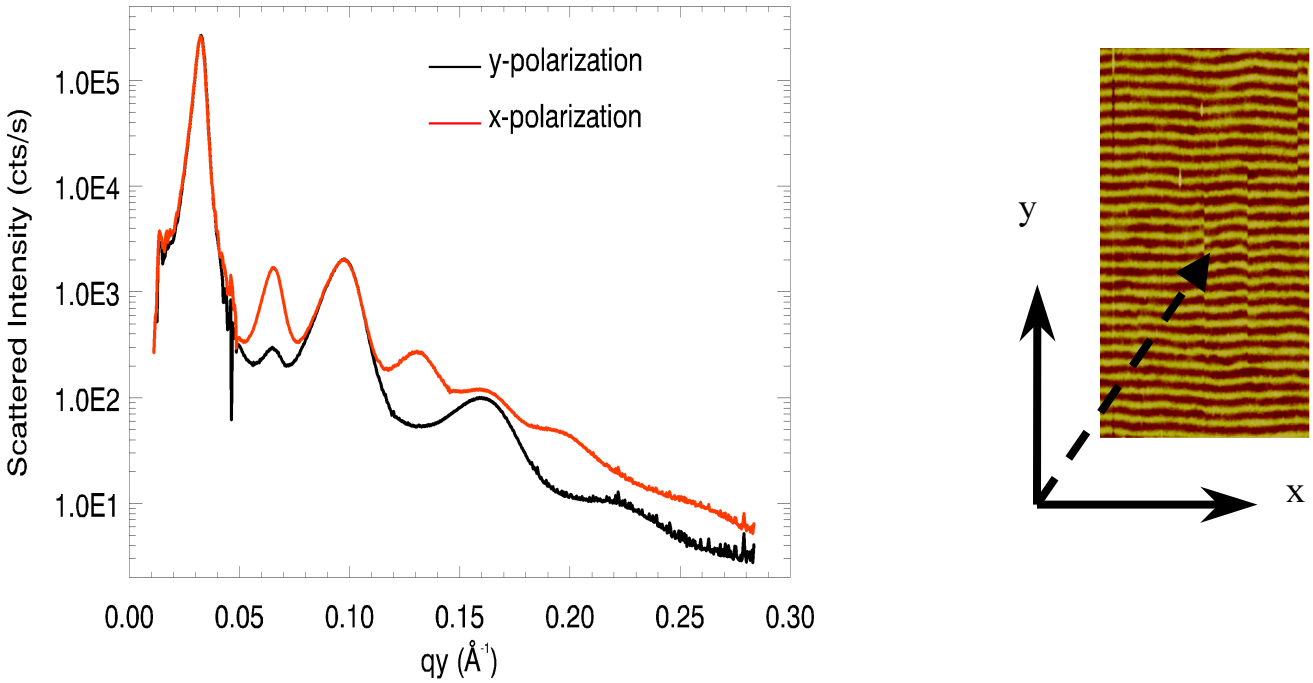

Fig. 5. Polarization dependence of the diffraction pattern in transmission of an ordered magnetic stripe lattice in amorphous $GdFe_5$ sample at 50 K. The image was taken at the maximum of the Gd resonance. Exposure time was 10 ms for the first order and 5 s for the higher orders. Up to nine diffraction orders are visible.

The complete diffraction patterns taken with horizontal and vertical polarizations are shown in Fig. 5 (Experiments with linear polarization became possible only on ID08, where the polarization can be made vertical or horizontal, and were obtained in Oct. 2001). Eight, possibly nine diffraction orders, corresponding to the Fourier components of the periodic structure, are visible.

These data can be understood in terms of the resonant dipole scattering amplitude [6]

$$f_{res}^{1} = \hat{\mathbf{e}}'\cdot\hat{\mathbf{e}}F^{(0)} - i(\hat{\mathbf{e}}' \times \hat{\mathbf{e}})\cdot\hat{\mathbf{M}}F^{(1)} + (\hat{\mathbf{e}}'\cdot\hat{\mathbf{M}})(\hat{\mathbf{e}}\cdot\hat{\mathbf{M}})F^{(2)}$$

where the three terms are a resonant charge term (F^0) with the same polarization dependence as the non-resonant Thomson scattering, and two terms proportional to the magnetization (F^1) and the magnetization squared (F^2). The vectors ê and ê' describe the polarization of the incident and scattered beam.

The GdFe films of our study are flat within 1 nm and homogeneous on length scales between 1 nm and several μm, implying that there is no scattering from the Thomson and F^0 terms. The resonant diffraction pattern is therefore the result of the two purely magnetic diffraction terms, and their interference. The F^2 term is weak at most resonances, but at the rare earth M edges can be comparable to F^1. As will be shown below, the presence of the F^2 term has the great advantage that one is sensitive to the three vector components of the magnetization.

If charge scattering can be ignored, in the limit of forward scattering the resonant scattering amplitude reduces to:

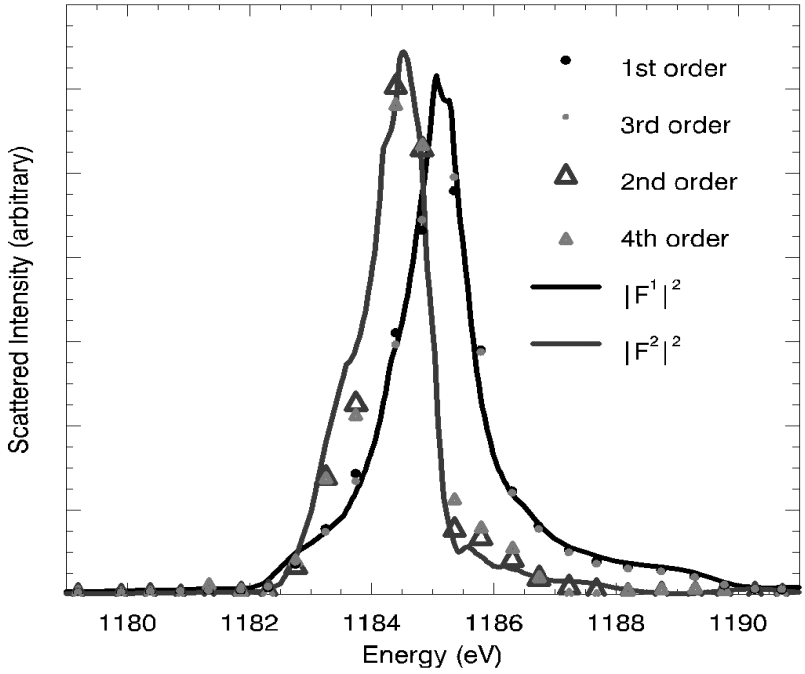

Fig. 6 Normalized intensity of even (circles) and odd (triangles) orders as a function of photon energy, taken with x-polarization. Solid lines: energy dependence of circular and linear scattering terms.

$$f_{res}^{1} = \begin{bmatrix} 0 & -iM_z \\ iM_z & 0 \end{bmatrix} F^{(1)} + \begin{bmatrix} M_x^2 & M_x M_y \\ M_x M_y & -M_y^2 \end{bmatrix} F^{(2)}$$

where linear polarization is assumed along the *x* or *y* axis and the light is incident along *z* (we follow the notation of Hill-McMorrow, the matrix elements give the amplitudes for scattering the vector (x,y) into the vector (x',y') [6]). It follows that at small angles the F^1 term is mainly sensitive to M_z while the F^2 term is sensitive to the in-plane components M_x (Bloch walls) and M_y (closure domains). With this expression, and ignoring interference terms between F^1 and F^2 terms for the moment, the diffraction patterns can be qualitatively understood.

The F^1 term sees the primary up-down stripe pattern $M_z(y)$ and produces a diffraction pattern with intensities given by the square of the Fourier components M_z^n of the magnetization M. A symmetric block wave magnetization would give only odd orders that are insensitive to polarization changes. An asymmetric block wave (*i.e.* up-domains larger than down domains or v.v.) would produce even orders. The F^2 term also produces mainly even orders, being proportional to products of magnetization components. However, the polarization selection rules makes this term sensitive only to in-plane magnetization components, to wit the Bloch walls (M_x) and the closure domains (M_y).

The origin of the even orders can be established definitively from the different energy dependence of the F^1 and F^2 scattering. In Fig. 6 the background-subtracted intensity of the first 4 orders is plotted as a function of photon energy. It is clearly seen that the uneven orders (circles) and even orders (triangles) have maximum intensities that differ by about 1eV. Furthermore, the data points follow the full curves representing the F^1 and F^2 contributions to the scattering cross section as obtained from XMCD and XMLD measurements (see below) very precisely.

Recapitulating, Fig. 5 can be understood as follows: the uneven orders are due almost exclusively to the out-of-plane domains. Polarization parallel to the horizontal stripe pattern illuminates the Bloch walls, while vertical polarization brings out the much weaker contribution from surface closure domains. The relative intensities, especially of the 1^{st} and 2^{nd} orders, reflect the total magnetization in the three directions, integrated over the film thickness. Thus, the huge dichroism of the second order implies that in this structure the total magnetization in the Bloch walls, M_x, is much larger than that in the closure domains. The absence of higher orders in the y-polarized spectrum signifies that the total y-magnetization has a simple sine structure, implying that their average width is about half the domain size. We surmise that in this state of the sample, *i.e.* after in-plane magnetization, the Bloch walls extend up to the surface, a state known as a *twisted domain wall state* [2]. The appearance of an 8^{th} order implies that this Bloch wall measures 25 nm (1/8 of the 190 nm period) or smaller. Clearly, this statement can be made more precise by fitting the data with a model magnetization structure.
In the next session we describe how the scattering strengths F^1 and F^2 can be determined from XMCD and XMLD measurements. These measurements were performed in October 2001, and their analysis has just been completed. With this knowledge, we will be able in the coming months to make the previous statements on the integrated magnetization components quantitative.

Spectroscopy

Quantitative determination of the M_{45} XAS, XMCD & XMLD spectra of Gd

We have measured the XAS, XMCD and XMLD transmission spectra on samples that were magnetically disordered, magnetized out-of-plane or in-plane respectively. Absolute cross sections could be obtained from the known efficiency of the detector. The absolute absorption cross sections are depicted in Fig. 7 and compared with calculations with the Cowan program showing an astoundingly *quantitative* agreement. These results show to our knowledge for the first time that the calculations not only predict the shape but also the *magnitude* of the spectra correctly.

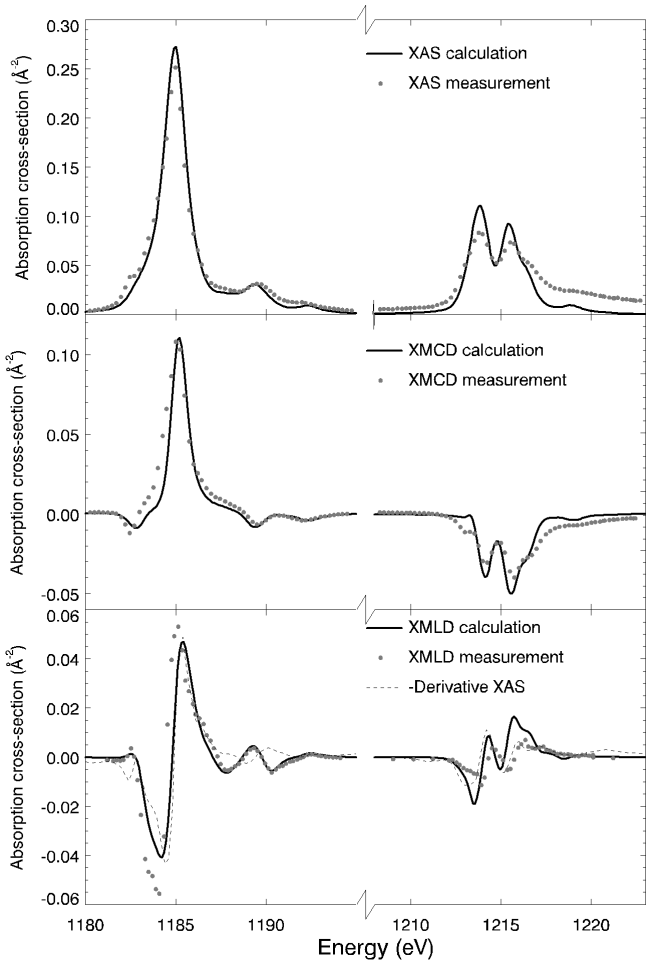

Fig 7. Quantitative XAS, XMCD and XMLD data for the M_{45} edge of Gd obtained from transmission experiments. Dots: experimental data. Full curve: calculated spectra [Cowan, Slater integrals reduced to 90%]. For comparison the derivative of the XAS is depicted in the lower XMLD panel.

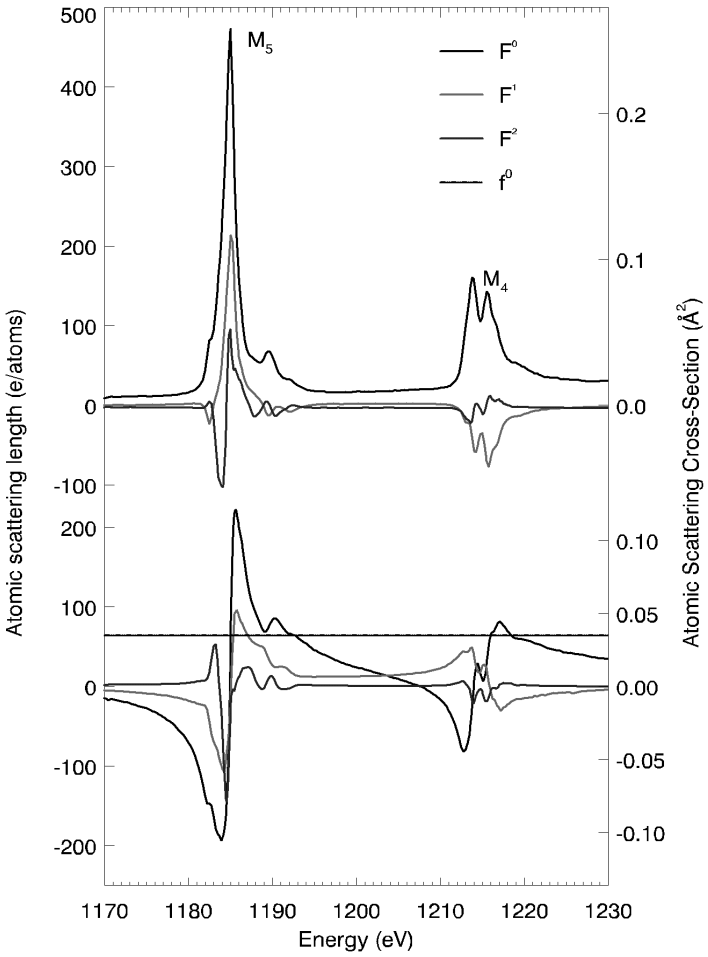

Fig. 8. Resonant scattering amplitude at the Gd M_{45} edges. Top: Imaginary parts of F^0, F^1, F^2. Bottom: Real parts obtained by Kramers-Kronig transform of the imaginary parts.

The Gd M_{45} resonant scattering cross section

The XAS, XMCD and XMLD spectra are proportional to the imaginary parts of the scattering factors F^0, F^1 and F^2. The corresponding real parts can be obtained from the Kramers-Kronig relations (note that in case of F^1 a modified transform has to be used [7]). The results are given in Fig. 8, and show that the imaginary and real contributions of F^1 reach values of 200 and 100 electrons/atom respectively and those of F^2 half of that. The right axis gives the approximate corresponding cross sections (obtained using a fixed value for the wavelength). Also indicated is the non-resonant high energy Thomson limit 65e.

This set of curves gives the complete energy dependence of the resonant scattering amplitude. As a test case we have measured the energy dependence of the total scattered intensity using a large area diode. Fig. 5 shows that this signal is coming almost exclusively from the 1st and 3rd harmonics, which we have shown above to be generated by F^1 terms. However, the scattered beams are reduced by the (polarization averaged) transmission factor and therefore

$$I_{scat} / I_{trans} \propto \left| F^1 \right|^2$$

This equality is tested in Fig. 9 where the dots represent the left-hand term obtained by dividing the angle integrated scattered intensity by the polarization averaged transmission spectrum, and the right-hand term is obtained by summing the squared F^1 curves of Fig. 8. Excellent agreement is obtained over 4 orders of intensity, showing that we have obtained the correct shape and ratio for the real and imaginary parts of F^1.

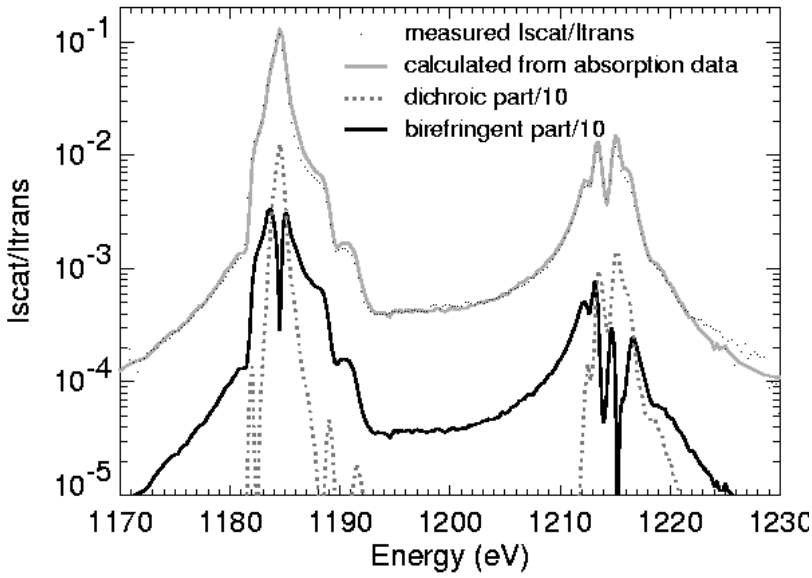

Fig. 9. Dots: intensity of first diffraction order normalized to transmitted beam (0th order) to account for absorption. Light line: Scattering cross section derived from the experimental XMCD data of Fig. 8. Bottom: The two contributions, offset by one order of magnitude. Dotted: imaginary part, full: real part.

Field dependence

In Fig. 2 the normalized magnetization curves for in-plane and out-of-plane magnetization were given. The in-plane loop is nearly linear in field for small M, and closes gradually for higher fields, without a recognizable saturation point. The out-of-plane loop on the other hand shows well-defined saturation and nucleation fields. Note that both cases show remanent magnetization.

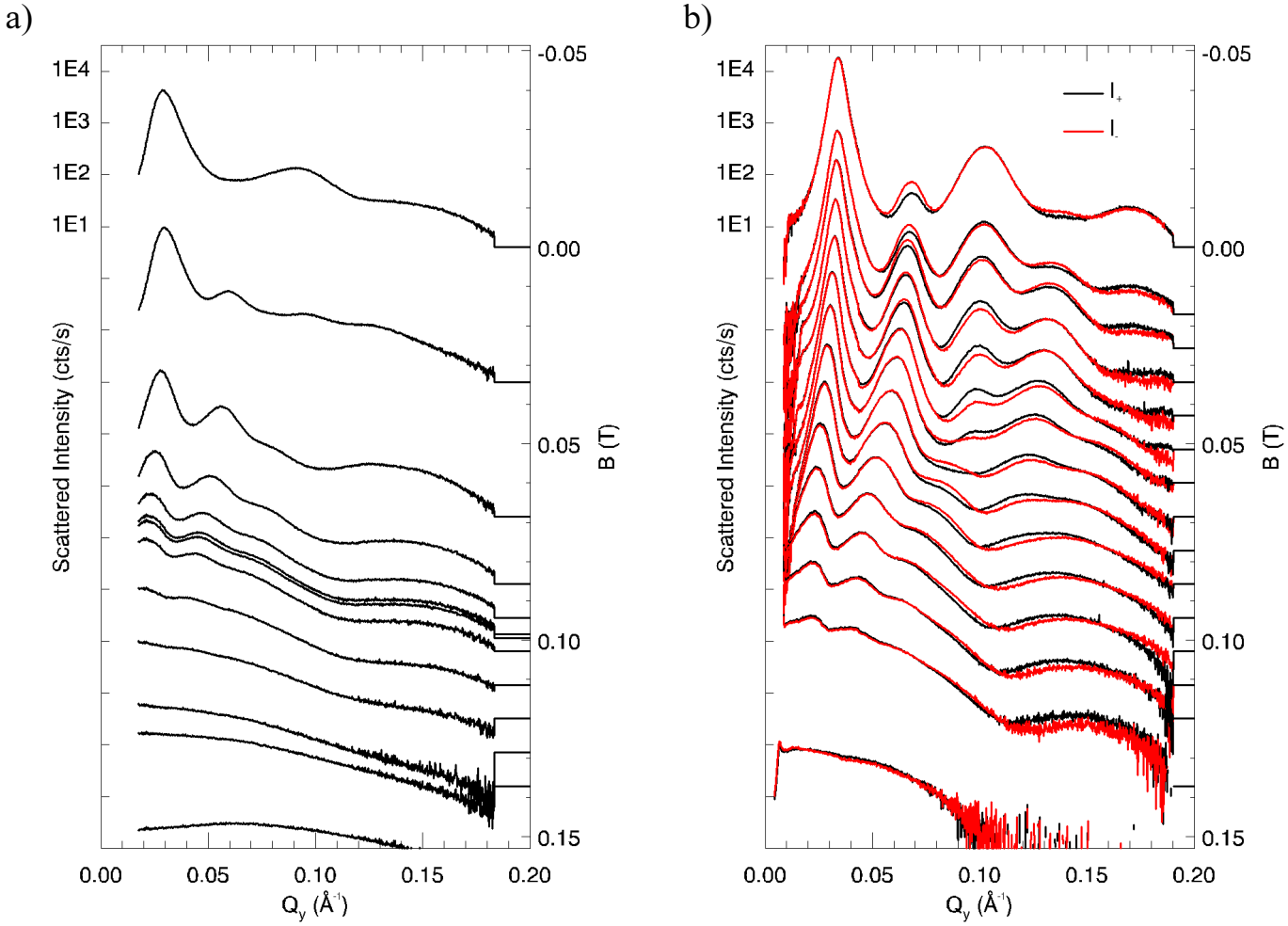

Fig. 10. a: Evolution of diffraction pattern of disordered stripes on applying a perpendicular field. The curves are offset by an amount corresponding to the field. b: Idem, starting from the aligned structure, red/black curves are for left/right circular polarized incident beam.

Fig. 10 shows the evolution of the diffracted intensity on applying a field normal to the film. At zero field only uneven orders are visible, due to the larger disorder, also reflected by the much larger peak widths. Furthermore, the period is about 30% larger than for the aligned stripes. On increasing the field, even orders appear, mainly due to the up-down asymmetry in the stripe magnetization induced by the field (F^1 term). The period is seen to increase rapidly with field

and a minimum develops at q=0.1 A^{-1}, which moves out to higher q with field. A magnetic signal remains to well above apparent saturation in the hysteresis loop.
Fig. 10b shows the same experiment starting from an aligned lattice, using circularly polarized light. Now at zero fields even orders are visible, which are strongly dichroic, due to interference between $F^2M_{x,y}{}^2$ terms and F^1M_z terms induced by the remanence of our magnet. For higher fields the alignment is washed out and again a minimum develops at q=0.1 A^{-1}. The broad structure can be interpreted as the form factor of the small reverse domains that survive to well above the apparent saturation field. From the position of the minimum their size can be estimated to be about 50 nm. The circular dichroic asymmetry of this scattering pattern shows that these reverse domains are still surrounded with in-plane magnetization structure from closure and Bloch walls.

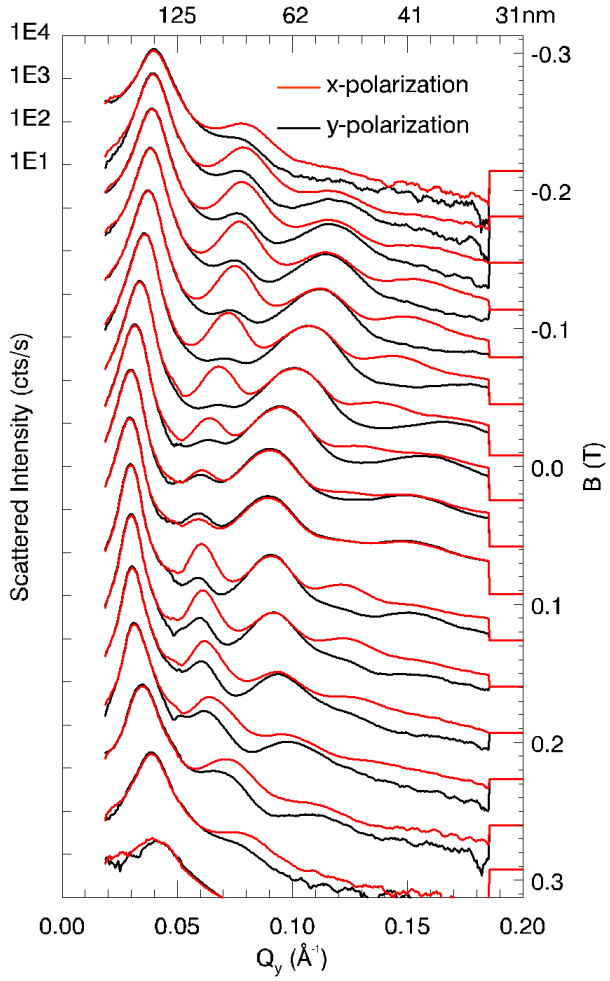

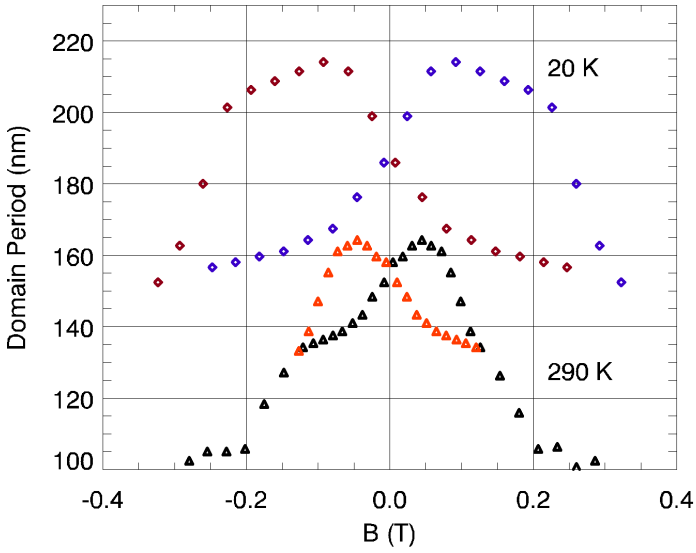

Fig. 11. Complete in-plane field scan from -0.3 to 0.3 Tesla, taken with linearly polarized light at 20 K. The 0 Tesla curves are the same as fig.5. (on left)

Fig. 12. Period as a function of in plane field. Shown are data for 20 K and 290 K (at top).

As another example, in Fig. 11 we present results for in-plane applied fields, now taken with linearly polarized light. The period, plotted in Fig. 12, is first seen to increase and then to decrease again, showing strong hysteresis. Near the maximum period, the even orders are

strongly reduced and their dichroism almost disappears, implying very little magnetization in the Bloch walls and closure domains. At high in-plane fields the Bloch walls, that have their magnetization in the direction of the field, grow in size. We can follow the scattered intensity over four orders of magnitude, to within a percent of saturation, showing the sensitivity of the technique.

Grazing incidence diffraction

Fig. 13 shows the same magnetization scan (field applied normal to the plane of the film, after stripes have been ordered by applying an in-plane field), but now taken in reflectivity using circularly polarized beams. The diffraction pattern disappears much faster than in the transmission case. Since in this geometry one is very sensitive to the coherence of the stripe pattern along the footprint of the beam, this indicates that during the domain movement the parallel alignment of the domains is gradually lost.

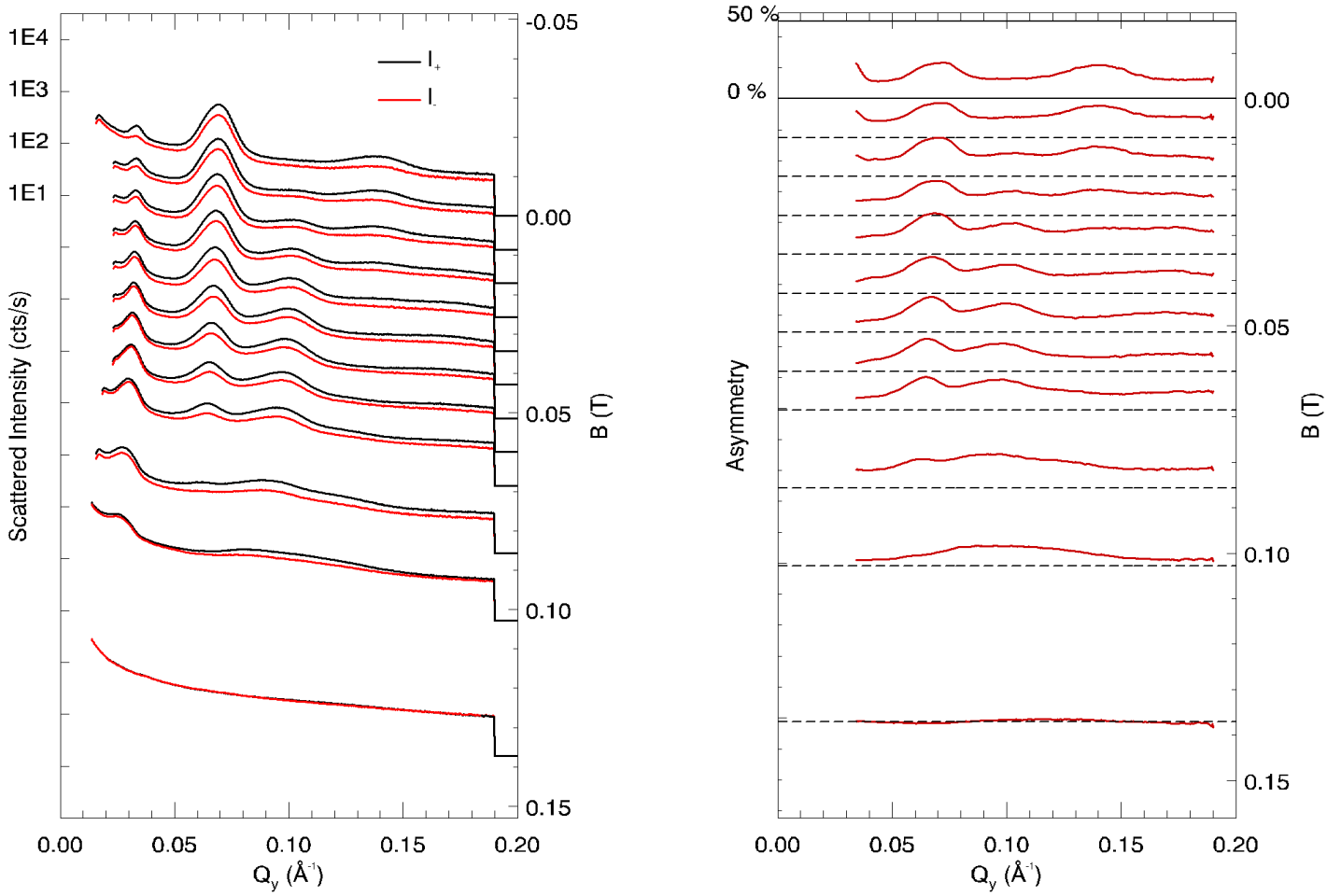

Fig. 13. Left: Evolution of diffraction pattern as a function of field applied normal to the film, taken in reflectivity with angle of incidence 3.5 degree. Right: Circular dichroic asymmetry.

The peak positions show the same behavior as found in the transmission data set: a gradual decrease to smaller q, and the development of a (weak) minimum at 0.1 A^{-1}. The intensities however are completely different. Firstly, in the remanent state the left and right circularly polarized spectra are offset over most of the spectrum, with an average asymmetry of ~20%, indicating that a substantial fraction of the surface is magnetized along the Bloch walls. The 2^{nd} and 4^{th} harmonics are very strong and the odd-orders, apart from the 1^{st}, order almost absent. For grazing incidence geometry, the polarization-dependent terms in the scattering formula give a totally different sensitivity to the three components of magnetization. The F^1 term is mainly sensitive to M_x , and the F^2 term to M_z^2, M_y^2 . These terms have half the periodicity of the up-down structure at 0 field, hence the strong even orders. The strong dichroic asymmetries observed are of a more complicated nature than in the transmission experiment. Not only there is interference between F^1 and F^2 scattering terms like in transmission, but also between scattering from bulk and closure-domain F^1 terms, the latter results in a left/right asymmetry as described by Dürr [8]. The energy dependence of the diffraction orders is therefore not as simple as that for the transmission case in Fig. 6.
On applying an "up" field that pushes the down domains apart, the even orders collapse, while the 1^{st} and 3^{rd} harmonics increase strongly, although remaining weaker than the original 2^{nd} order.
Fig. 13 is one of several data sets. The diffraction patterns taken in reflectivity are extremely sensitive to the angle of incidence, and the interpretation is further complicated by the presence of circular and linear dichroic extinction.

Coherent diffraction and magnetic x-ray speckle

For the development of magnetic dynamical light scattering, stable coherent beams with sufficient intensity are a prerequisite. In this section we discuss the coherence requirements and how they can be set and determined.

Longitudinal coherence

The longitudinal coherence length (the distance over which a half-period phase difference builds up between the lowest and highest wavelengths present in the beam) is determined by the bandwidth of the beamline. For the experiments performed here, the requirement is that the coherence length be longer than the correlation lengths of the structure studied. At the highest resolution of the beamline it is of the order of 20 μm. In transmission experiments the sample thickness is ~30 nm, much smaller than this. In reflectivity experiments, the correlation length of the sample over the footprint is not relevant since we are looking at transverse correlations. No special efforts are necessary to generate sufficient longitudinal coherence.

Transverse coherence, Fraunhofer diffraction

We have characterized the transverse coherence length of ID12B using the Airy diffraction patterns of high quality pinholes of 10 μm diameter. An example is given in Fig. 14, obtained with a pinhole screen distance of 2 m and a 10x microscope objective on the CCD camera. At least 23 diffraction orders can be counted, showing that the coherence length in both transverse directions is over 10 micron. Patterns like this can be obtained routinely by reducing the vertical divergence of the beam to 50% just after the refocusing mirror. The coherent intensity is roughly given by the ratio of the pinhole area over the total focal spot size (25x600 μm). Therefore the maximum coherent flux is 0.3-0.6% of the total intensity. Horizontal focussing could improve this somewhat. A more detailed analysis will appear elsewhere.

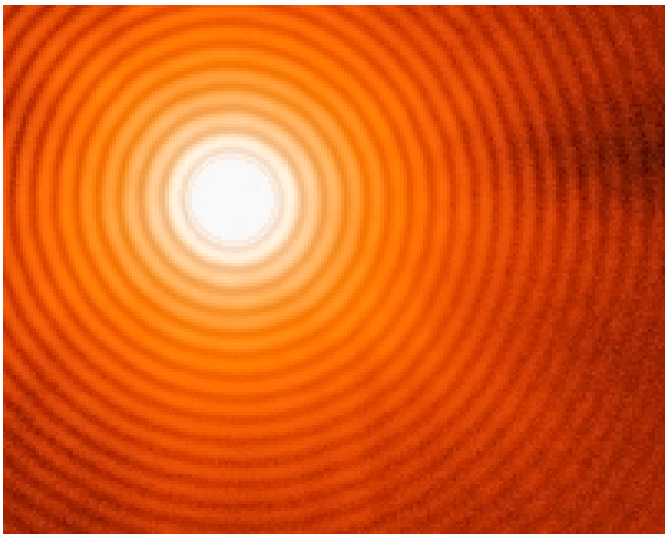

Fig. 14. Airy pattern obtained in the far field of a 10 μm diameter pinhole in the vertical focus of ID12B at an energy of 1000 eV.

For a typical soft x-ray coherence experiment one aims at studying sample correlation lengths from the wavelength upwards to ~10 μm, in order to create a comfortable overlap with optical laser wavelengths. The coherence of the beam line is therefore very satisfactory for most experiments.

X-ray magnetic speckle

Fig. 15 shows the first order diffraction spots of magnetically aligned stripes as in Fig 4, right, using a 10 μm coherent beam, as witnessed by the Airy rings around the primary beam shown in the middle. Both diffracted beams have split up in a well-defined speckle pattern with each speckle having the size of the central Airy disk (although it appears larger due to the overexposure necessary to bring out the Airy rings). The speckle peak-to-valley contrast is ~85%, as is typical for a dense speckle pattern.

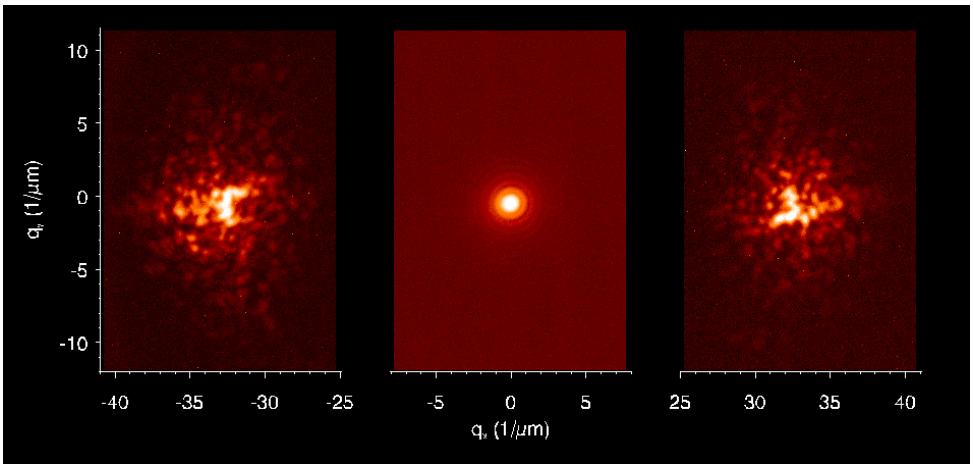

Fig. 15. First order resonant diffraction peaks of aligned stripes in $GdFe_5$ taken at the Gd M_5 resonance and using a coherent beam.

For the 1st order, the scattered intensity can be written as

$$I(q) \propto \left| \int F^1 \, M_z(y) e^{-iqy} dy \right|^2$$

These speckle patterns reflect the details of the disorder in the stripe lattice $M_z(y)$ over the illuminated area of 10 μm diameter. Indeed, after briefly saturating the sample the speckle pattern is completely different, corresponding to a different realization of $M_z(y)$. We stress here again that in our experiment we do not have any charge scattering: on saturating the sample all diffracted intensity disappears. We can therefore conclude that our data show x-ray speckle of purely magnetic origin.

It is worth pointing out that the two patterns have a high degree of inversion symmetry. This can be directly seen by following the main Γ shape on the left hand image. More quantitatively, the spatial correlation coefficient after rotating by 180° is 0.93. Inversion symmetry of *I(q)* is indeed expected because in the absence of charge scattering

$$I(q) \propto \left| F^1 \right|^2 \left| \int M_z(y) e^{-iqy} dy \right|^2$$

implying that $I(q) = I(-q)$, since M_z is a real number.

The speckle image was taken on ID12B and required a 500 s exposure with our 3% efficient detector. On ID08 the intensity at the Gd M_5 edge is at least 20x higher. A pixel detector with a quantum efficiency of 1 should allow one to follow the speckle pattern at video rates.

An x-ray lens would transpose the speckle image to a diffraction-limited image of the stripe image, with a resolution given by the diffraction order, 180 nm in this case. This shows that all spatial correlations between 180 nm and the beam diameter, 10 μm, are present in these speckle images. In the diffraction experiment one looses the phase information, and direct image reconstitution is not possible. A simple Fourier Transform (Fig. 16) of the speckle image however shows the main correlations in the illuminated area. It shows the stripe positions

modulated by the overall correlation function. The size of the bright correlated regions is of the order of 3 μm both along the stripes and perpendicularly to them.

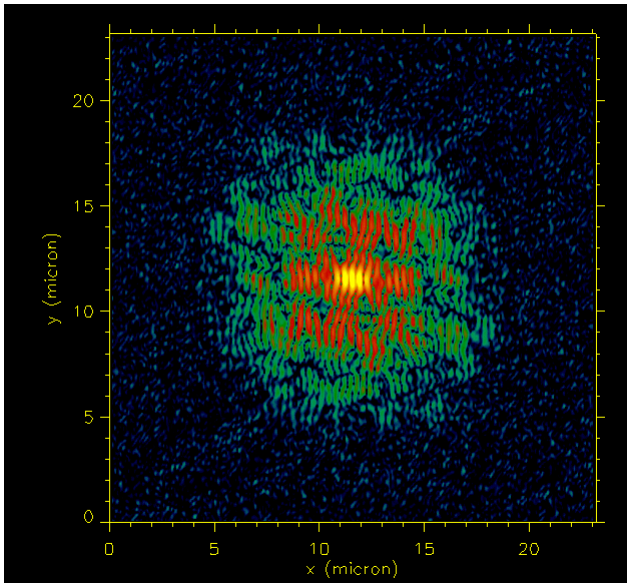

Fig 16. Spatial correlations of the magnetization over the illuminated area obtained by Fourier transforming the speckle image.

Methods exist [9] to recover the phase information using a known geometrical constraint such as the shape of the illuminating beam. Although this will give the same information as the MFM picture, we are working on applying these methods.
The important point of this study however is that it shows that is possible to obtain high speckle contrast as required for dynamical light scattering studies. The speckle intensity seems sufficient for such studies, at least for strong resonances as Gd. The next step in this development is to see whether the beamline temporal stability is sufficient. ID12B was not particularly stable and these tests were postponed till the migration of the beamline to ID08, and are now foreseen for July 2001.

Conclusion

With our experiments on the model system *a*-$GdFe_5$ we have explored the possibilities for studying the magnetic structure of thin films and surfaces with high resolution. We have shown the power of different combinations of field and circular or linear polarization. It should be clear from the above discussion that the proposal has been very successful experimentally. A huge amount of high quality data has been obtained, thanks to the possibility offered by the long term proposal construction to do systematic development of experimental technique and instrumentation. A substantial fraction of the data still has to be analyzed in detail. We have shown how the combination of transmission and reflectivity experiments allow one to obtain very detailed information on the behavior of stripe domains during the magnetization loop. In doing so we have demonstrated the power of resonant soft x-ray diffraction that is complementary to imaging techniques. Most imaging techniques are only sensitive to the stray field above the sample (MFM) or to the surface (SP-STM). Lorentz microscopy is probing the

bulk, but is incompatible with magnetic fields. RXMS has shown itself to be very flexible, both in field geometries and temperatures, and can be very efficient when 2D detectors are used.
We have started to explore the use of coherent x-rays for the generation of magnetic x-ray speckle, a phenomenon not existing in the visible spectral range. We have obtained very high quality speckle patterns that are highly centrosymmetric. We have studied the resonant character of these patterns, finding good correlation of the pattern over the M_4 and M_5 edges. This is explained by the fact that the phase field has the same shape as the amplitude field at the back of the sample, leading to the absence of MAD effects. Such effects will exist only if there is a charge structure that differs from the magnetic structure.
Our speckle results open the possibility to do phase retrieval to work back to the sample structure. More exciting is the possibility to mix the speckle information with a reference beam in order to produce true holographic images.
Finally we have started to exploit the speckle information in critical scattering experiments on Gd thin films. The first steps are encouraging, showing that we have mK temperature resolution and that we can follow the magnetization to within mK of the critical point. However, this remains a very challenging experiment, requiring extremely high quality Gd surfaces. Another way of studying dynamics, on much shorter time scales, has been started in a separate proposal where the time structure of synchrotron radiation is used to study magnetization reversal on nanosecond time scales and nanometer resolution.

References

[1] J.F. Peters, M.A. de Vries, J. Miguel, O. Toulemonde and J.B. Goedkoop, Magnetic Speckles with Soft X-rays, *ESRF Newsletter* **34** (2000) 15-16
[2] A. Huber and Rudolf Schäfer, *Magnetic Domains*, (Springer Verlag ,1998)
[3] C. Kooy and U. Enz, *Philips Res.Repts*. **15**,7-29 (1960)
[4] C. Kittel, *Phys. Rev.* **71**,965-971 (1946)
[5] W.F. Brown Jr.,*Micromagnetics*, (Wiley, 1963), J. F. Löffler, H.-B. Braun, and W. Wagner, Phys. Rev. Lett. **85**, 1990-1993 (2000)
[6] J.P Hannon, G.T. Trammel, M. Blume and D. Gibbs, *Phys. Rev Let*., **61**, 1245-1248 (1988), J.P Hill and D.F. McMorrow, *Acta Cryst. A,* **52**,236-244 (1996)
[7] D. Y. Smith, *Phys. Rev. B* **13**, 5303 (1976).
[8] H.A. Dürr, E. Dudzik, S.S. Dhesi, J.B. Goedkoop, G. van der Laan, M. Belakhovsky, C. Mocuta, A. Marty and Y. Samson, Science **248,** 2166-2167 (1999)
[9] R.W. Gerchberg and W.O. Saxton, *Optik.,* **35**, 237-246 (1972), Jianwei Miao, Pambos Charalambous, Janos Kirz, David Sayre, Nature **400**, 342 - 344 (1999)

Appendix: Experimental runs and participants

Proposal	Period	Beamline	#shifts	Subject
HE623	August 1999	ID12B	6	Characterization of coherence of beamline, Fraunhofer diffraction
HE623	November 1999	ID10A	18	Characterization of diamond phase plate
HE623	December 1999	ID12B	15	Magnetic diffraction in reflectivity (ESRF 7 Tesla magnet)
HE623	March 2000	ID12B	12	First coherent diffraction experiments
HE623	June 2000	ID10A	18	Magnetic diffraction Gd L_{23} edge influence of phase plate on coherence
HE623	July 2000	ID12B	18	Coherent diffraction
HE623	November 2000	ID12B	18	Field and polarization dependent scattering
HE623	July 2001	ID08	18	Commissioning of Bertha diffractometer Magnetic scattering in reflectivity Critical scattering on Gd crystal surfaces
HE1099	September 2001	ID08	18	Linear dichroism measurements Magnetic scattering in transmission using linearly polarized light

Collaborators

Dr. J.B. Goedkoop, Assistant Professor, University of Amsterdam
J.F. Peters, Ph.D. FOM
M.A. de Vries, Ph.D. FOM, October 1999 - January 2002
J. Miguel Soriano, Ph.D. FOM January 2000, based at ESRF from February 2002
Prof.Dr. J.F. van der Veen, University of Amsterdam/SLS Villingen
J.H.H. Bongaerts, Ph.D. FOM, University of Amsterdam
Dr. O. Toulemonde, Post-Doc January 2000 - December 2001
H. Luigjes, Technician, University of Amsterdam

Local contacts ESRF

ID12B/ID08: Dr. N.B. Brookes, Dr. S. Dhesi
ID10A: Dr. Carsten Detlefs